

Portland State University

PDXScholar

Civil and Environmental Engineering Faculty
Publications and Presentations

Civil and Environmental Engineering

2-2022

A Self-Referencing Non-Destructive Test Method to Detect Damage in Reinforced Concrete Bridge Decks Using Nonlinear Vibration Response Characteristics

Ali Hafiz

Portland State University, hafiz@pdx.edu

Thomas Schumacher

Portland State University, thomas.schumacher@pdx.edu

Anis M. Raad

Valar Consulting Engineering

Follow this and additional works at: https://pdxscholar.library.pdx.edu/cengin_fac



Part of the [Civil and Environmental Engineering Commons](#)

Let us know how access to this document benefits you.

Citation Details

Published as: Hafiz, A., Schumacher, T., & Raad, A. (2022). A self-referencing non-destructive test method to detect damage in reinforced concrete bridge decks using nonlinear vibration response characteristics. *Construction and Building Materials*, 318, 125924.

This Pre-Print is brought to you for free and open access. It has been accepted for inclusion in Civil and Environmental Engineering Faculty Publications and Presentations by an authorized administrator of PDXScholar. Please contact us if we can make this document more accessible: pdxscholar@pdx.edu.

1 **A Self-Referencing Non-Destructive Test Method to Detect Damage**
2 **in Reinforced Concrete Bridge Decks Using Nonlinear Vibration**
3 **Response Characteristics**

4
5 Ali Hafiz¹, Thomas Schumacher^{2,*}, and Anis Raad³

6
7 ¹ PhD, Senior Engineer, Advanced Infrastructure Design, Inc., Hamilton, NJ,

8 E-mail: ahafiz@aidpe.com

9 ² PhD, PE (DE), Associate Professor, Civil and Environmental Engineering, Portland State

10 University, Portland, OR, E-mail: thomas.schumacher@pdx.edu

11 ³ M.S., EIT Engineer, VALAR Consulting Engineering LLC, Clackamas, OR, E-mail:

12 anis.raad@valarengineering.com

13
14 *Corresponding Author

15
16 Abstract: Several non-destructive test (NDT) methods, namely visual inspection, hammer
17 sounding, chain drag, impulse response testing, impact echo testing, ultrasonic (array) echo testing,
18 and under certain conditions ground penetrating radar (GPR) are currently used to detect and
19 estimate the extent of damage such as delaminations in reinforced concrete bridge decks. In this
20 article, we present a self-referencing NDT method that builds on impulse response (IR) testing to
21 detect damage using nonlinear vibration characteristics. The hypothesis is that for an undamaged

22 deck, varying the impact force applied to a specific test point does not affect the corresponding
23 frequency response function (FRF) for frequencies that lie within the measurement system's linear
24 operating range. On the other hand, the FRFs for a test point that contains damage changes when
25 the impact force is increased, indicating a nonlinear vibration response. To demonstrate that the
26 concept works theoretically, two 2D finite element (FE) models of a bridge deck, one containing
27 a shallow delamination, were developed and their responses to impact forces of increasing
28 amplitude compared. IR data from an in-service bridge deck was processed and analyzed. Visual
29 inspection results and ultra-high-pressure hydro-blasting performed on the deck for rehabilitation
30 purposes provided an opportunity to compare the obtained results with common inspection
31 methods and actual damage extent. Based on the observations, a new damage index, referred to as
32 nonlinear vibration index (NVI), is proposed and shown to be sensitive to damage, including
33 shallow delaminations that were missed by means of visual inspection.

34
35 **Keyword:** Bridge deck; reinforced concrete; damage detection; delamination; condition
36 assessment; non-destructive testing; impulse response testing; nonlinear vibration characteristics;
37 frequency response function; finite element model.

39 **1. Background and Motivation**

40 Highway infrastructure in the United States and around the world experience degradation due to
41 environmental conditions and increasing traffic volume. Additionally, damage is caused by
42 degradation of structural materials due to aging. The corrosion of steel bars and resulting gradual
43 degradation of the concrete are the most common causes of damage in reinforced concrete

44 structures (NCHRP 2004). Accordingly, bridge engineers are typically concerned about four
45 primary damage mechanisms: steel reinforcing bar (or rebar) corrosion, delamination, vertical
46 cracks, and concrete degradation (Gucunski, Imani et al. 2013). Delaminations in concrete bridge
47 decks, which are the focus of this article, are an advanced form of damage in reinforced concrete
48 bridge decks resulting from advanced corrosion of the embedded steel rebar, and are initiated by
49 the presence of cracks in the concrete and sufficient moisture. The rebars expand due to corrosion,
50 leading to cracking and subsurface fracture planes within the concrete. With advancing corrosion,
51 delaminations can progress to open spalls.

52
53 To date, many non-destructive test (NDT) methods have been developed to detect deterioration in
54 concrete bridge decks such as delaminations (Scott, Rezaizadeh et al. 2003, Arndt, Schumacher et
55 al. 2011, Zhang, Harichandran et al. 2012, Gucunski, Imani et al. 2013, Sun, Zhu et al. 2018,
56 Garrett 2019). An ultrasonic stress pulse is used in techniques aiming to initiate high-frequency
57 stress waves, which include impact echo (IE) and ultrasonic echo (UE) testing (Sansalone and
58 Streett 1997, Kee, Oh et al. 2012, Zhang, Harichandran et al. 2012, Shokouhi, Wolf et al. 2014,
59 Scherr and Grosse 2021). On the other hand, low-frequency dynamic response characteristics are
60 used in impulse response (IR) testing (Davis 2003). In the latter method, specific characteristics of
61 the dynamic response to a given hammer impact are evaluated to detect delaminations among other
62 degradations. IR testing is based on a hammer impact resulting in a low strain stress wave and
63 vibrations and it has been primarily used for pile integrity testing (Davis and Robertson 1975).
64 While the methodology of this test has not changed since its popularization in the 1970s,
65 application to other types of concrete members has increased notably (Davis 2003, Davis and
66 Germann Petersen 2003, Sajid and Chouinard 2019). ASTM Standard C1740 provides guidance

67 for evaluating the condition of concrete plates such as bridge decks using the IR method (ASTM
68 2016). In IR testing, an instrumented hammer is struck against the concrete surface to generate
69 local vibrations, and the dynamic response is measured at a nearby location using a geophone or
70 accelerometer. The frequency response function (FRF) is obtained by dividing the dynamic
71 response by the impact force, where both signals are expressed in the frequency domain. The
72 typical frequency range used to evaluate the condition of a concrete slab is 0 to 1 kHz (ASTM
73 2016). Several parameters are computed from the FRF, referred to as mobility plot, that are used
74 as empirical indicators of damage. For concrete bridge deck condition assessment, all available
75 NDT technologies have limitations to identify certain types of defects (Abdelkhalek and Zayed
76 2020). One of the limitations of the IR method is that it cannot detect defects with a large depth-
77 to-size ratio (Lin, Azari et al. 2021). Moreover, limitations in detecting delaminations of a certain
78 size appear to be related to the fixed frequency limit prescribed by the ASTM standard (Clem,
79 Popovics et al. 2013). Finally, the method may not be sensitive to early stages of damage because
80 it solely relies on linear response characteristics.

81
82 In structural dynamics, modal analysis is the most popular approach for performing linear-elastic
83 structural system identification, where the modal parameters, i.e., natural vibration frequencies,
84 mode shapes, and damping ratio, can be extracted and monitored over time (Kerschen, Worden et
85 al. 2006, Farrar and Worden 2013). Since these parameters are a function of the structural and
86 material properties, they can be related to the initiation and propagation of damage (Doebling,
87 Farrar et al. 1998). Samman and Biswas (Samman and Biswas 1994, Samman and Biswas 1994)
88 presented waveform-recognition techniques to detect damage in bridges and they applied these
89 techniques under both laboratory and real-world conditions by detecting damage in a laboratory-

90 sized bridge and a highway bridge. These techniques depend on a comparison between two
91 dynamic signatures: one from an intact (= reference) state and the other from a state with a certain
92 level of damage. Zhou et al. (Zhou, Wegner et al. 2007) utilized vibration-based damage detection
93 (VBDD) methods to detect and localize low levels of damage in the deck of a two-girder, simply-
94 supported bridge. They conducted their study using laboratory-based experimental and finite
95 element analysis. The methods evaluated included the mode shape curvature method, the change
96 in flexibility method, the damage index method, the change in uniform flexibility curvature
97 method, and the change in mode shape method. They concluded that VBDD methods have
98 excellent potential as structural health-monitoring tools for bridge decks. However, these methods
99 require extracting the mode shapes, a process requiring multiple sensors. Additionally, there is
100 difficulty in extracting the mode shapes for bridge decks in the field (Salawu and Williams 1995,
101 Bien, Krzyzanowski et al. 2002) because the excitation forces are required to have sufficiently
102 large amplitudes (Bien, Krzyzanowski et al. 2002). Kee et al. (Kee and Gucunski 2016) used
103 impact-echo (IE) testing in order to improve the interpretation of local flexural vibration modes of
104 delaminated areas in concrete bridge decks. This approach was more accurate than conventional
105 binary images for detecting the areal sizes of shallow delaminations. On the other hand, for deep
106 delaminations, the conventional IE approach was more accurate (Kee and Gucunski 2016). Finally,
107 there are two challenges in using modal analysis methods for damage detection: first, it requires
108 the dynamic response for the reference case, which is unavailable in most cases. Second,
109 temperature variations can have a significant effect on the frequency response of the structure
110 (Zhou, Ni et al. 2011), and there might be significant difficulty in distinguishing between the
111 effects of temperature and damage.

112 Fundamentally, if a structural system fails to follow the principle of superposition, i.e., its response
113 deviates from linearity, then it can be considered nonlinear (Ewins 1995), and traditional linear-
114 elastic modal analysis cannot be used to analyze the dynamic response. In reality, most structural
115 systems exhibit a certain level of nonlinear behavior (Lin 1990). The sources of nonlinearity can
116 be summarized as (Farrar and Worden 2013): (1) Geometric nonlinearity, when the structure
117 exhibits large displacements, (2) material nonlinearity, when a material exhibits a nonlinear stress-
118 strain response, (3) nonlinear boundary conditions, where imperfect boundary conditions result in
119 a nonlinear vibration response, (4) damage, for example cracking, and (5) energy dissipation due
120 to damping. This last phenomenon is to date not fully understood. According to Samman and
121 Biswas (Samman and Biswas 1994), the identification of nonlinear behavior of a structural system
122 includes three steps. The first step is “Detection,” where the existence of nonlinearity in structural
123 behavior is determined. “Characterization” is the second step, where the source and location of the
124 nonlinearity is investigated, and its behavior established. The final step is “Parameter estimation.”
125 In this step, the coefficients of the nonlinearity are estimated, and their uncertainty quantified.
126 There are many identification methods that have been established in the preceding three decades,
127 such as the restoring force surface method and nonlinear autoregressive moving average model
128 with exogenous inputs (NARMAX) method (Kerschen, Worden et al. 2006, Noel and Kerschen
129 2017). Nonlinearity is important in damage detection for cases where damage changes the behavior
130 of the structural form (initially) from linear to nonlinear (Lin 1990). Underwood et al. (Underwood,
131 Meyer et al. 2015) investigated using nonlinear behavior for detecting and locating subsurface
132 damage in composite materials by comparing the FRFs for different input force amplitudes. Idriss
133 et al. (Idriss, El Mahi et al. 2015) found that nonlinear vibration parameters are much more
134 sensitive to debonding damage in sandwich beams than linear vibration parameters. Zhao et al.

135 (Zhao, Lang et al. 2015) presented a new transmissibility analysis method for the detection and
136 location of damage using the characteristics of nonlinear vibrations of structural multi-degree-of-
137 freedom (MDF) systems.

138

139 This literature review reveals an opportunity to improve the sensitivity of the established IR test
140 method to detect delaminations in concrete bridge decks early on. The objective of this study was
141 thus to develop and evaluate a highly sensitive yet simple NDT test method to detect damage such
142 as delaminations in reinforced concrete bridge decks. Unlike traditional vibration-based methods,
143 the method discussed herein is self-referencing, i.e., it does not require a reference measurement
144 of the undamaged state for comparison. Using the impulse response (IR) test procedure, the
145 collected data is analyzed in a manner that enables us to detect damage based on deviation from
146 linearity, following what was originally proposed by Ewins (Ewins 1995), i.e., by comparing the
147 frequency response functions (FRF) due to impacts of varying amplitude. The significance of the
148 proposed method lies in its availability, simplicity, cost-effectiveness, and that its application could
149 be extended to other members.

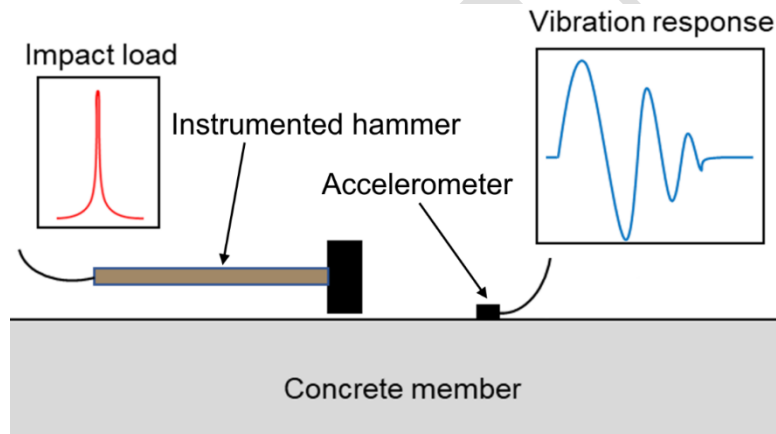
150

151 **2. Test Methodology**

152 The proposed method is based on the vibration response of a reinforced concrete bridge deck and
153 produces a nonlinear vibration index (*NVI*) for each test point on the member. The same
154 instruments and general test procedure used for impulse response (IR) testing and vibration-based
155 methods apply: An instrumented hammer is used to create an impact at a specific test point and
156 the vibration response at a nearby location is measured with an accelerometer (see Fig. 1). The

157 proposed method requires applying at least two impact forces with different amplitudes for each
158 test point and measuring their vibration responses separately. The basic concept is that for a test
159 point on an ideal undamaged linear-elastic structural system, varying the amplitude of the impact
160 force does not result in a change in the FRF. On the other hand, a test point on a system that
161 contains damage exhibits nonlinear characteristics, which result in different FRFs for impact forces
162 of different amplitude. The frequency ranges of the FRFs need to be within the linear operating
163 range of the measurement system.

164



165

166 **Fig. 1.** Illustration of test setup used in this study.

167

168 A parameter describing the nonlinearity effect, or deviation from linearity, can be computed in
169 multiple ways, see e.g., Idriss et al. (Idriss, El Mahi et al. 2015), Zhao et al. (Zhao, Lang et al.
170 2015) and Liu et al. (Liu, Todd et al. 2017). Typically, the correlation coefficient or root mean
171 square are used. Assuming two different impact forces (e.g., soft and strong), our proposed *NVI* is
172 computed for each test point as follows:

173
$$FRF = H(f) = \frac{Y(f)}{X(f)} = \frac{G_{xy}(f)}{G_{xx}(f)} \quad (1)$$

174
$$COV(H_0, H_i)(f) = \frac{1}{f-1} \sum_{j=1}^f (H_0 - \mu_{H_0})(H_i - \mu_{H_i}) \quad (2)$$

175
$$\rho_{H_0, H_i}(f) = \rho(f) = \frac{COV(H_0, H_i)(f)}{\sigma_{H_0} \sigma_{H_i}} = \frac{\sigma_{H_0, H_i}}{\sigma_{H_0} \sigma_{H_i}} \quad (3)$$

176
$$R^2(f) = \rho(f)^2 \quad (4)$$

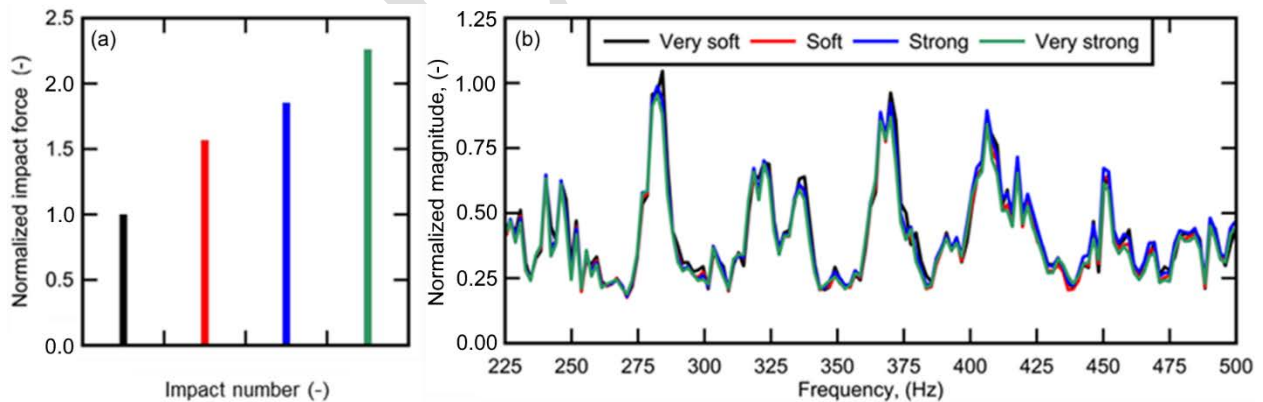
177
$$NVI = \frac{\sum_{f_1}^{f_2} R^2(f)}{f_2 - f_1} \quad (5)$$

178

179 where $Y(f)$ and $X(f)$ are the frequency domain representations of the measured vibration response
 180 and the impact force, respectively, and H_0 and H_i are the FRFs associated with two impact forces
 181 having different amplitudes. In this study, the FRF associated with the lowest force of a set of
 182 measurements from a particular test point was assigned to H_0 , representing the reference case.
 183 $COV(H_0, H_i)$ is the covariance between H_0 and H_i , and μ indicates mean values. ρ is the correlation
 184 coefficient, f_1 and f_2 are the lower and upper limits of a selected frequency range, respectively. G_{xy}
 185 is the cross spectrum between the measured vibration response and the impact force and G_{xx} is the
 186 auto spectrum of the measured impact force. NVI is the proposed nonlinear vibration index and a
 187 scalar between 0 and 1, indicating the level of nonlinearity in the structural system under
 188 evaluation. When $H_0 = H_i$, then $NVI = 1$, implying the structural system behaves linearly;
 189 otherwise, the FRFs are different, which implies that the structural system exhibits a certain level
 190 of nonlinearity.

191

192 In our proposed method, a test point on a bridge deck without damage is assumed to represent an
 193 ideal linear-elastic structural system, i.e., the FRF does not change with an increase in the
 194 amplitude of the impact force. This is illustrated in Fig. 2, where the FRFs of four impact forces
 195 with increasing amplitude [Fig. 2 (a)] are shown for test point A1 [see Fig. 9 (a)] on the tested
 196 bridge deck (introduced in Section 5.1). From Fig. 2 (b), it can be observed that increasing the
 197 applied impact force, even doubling it, does not result in significant visible differences between
 198 the FRFs, indicating system linearity, which in turn implies that no damage is present in the system.
 199 Our hypothesis is that if any area of a bridge deck deviates from linearity, some type and level
 200 damage can be assumed to be present. The observed nonlinearity is assumed to be caused by
 201 cracking and crack boundary interaction. Note that all other potential sources of nonlinearity must
 202 be controlled, i.e., minimized (see Section 5.3). Also, the selected frequency range ($f_1 = 225$ to f_2
 203 $= 500$ Hz) was determined by trial and error and is application dependent. More details are
 204 provided in Section 5.2.

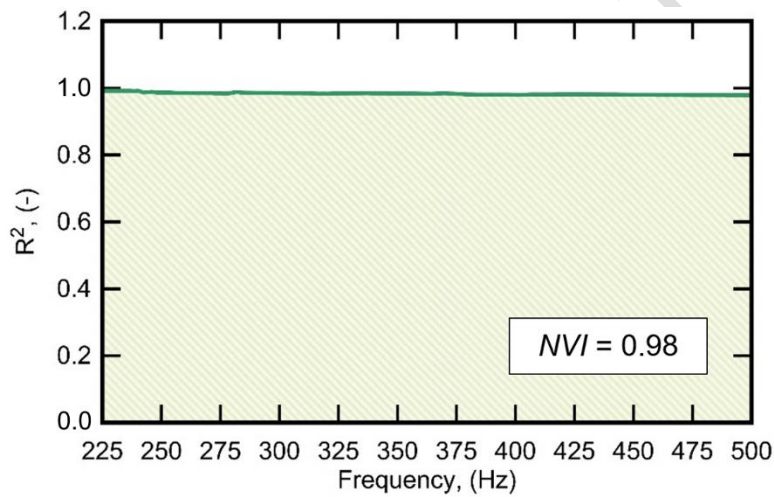


206
 207 **Fig. 2.** Sample FRFs for test point A1 [see Fig. 9 (a)] on the selected bridge deck.

208

209 Fig. 3 shows a sample of the coefficient of determination, R^2 as a function of frequency. This
210 coefficient was determined by comparing the FRFs of the very soft and very strong impact forces
211 shown in Fig. 2 (b). Finally, the normalized area under the coefficient of determination-frequency
212 curve represents the NVI , which for this case is 0.98. This value confirms that the system shows a
213 very high degree of linearity at this test point, which was consistent with visual inspection results.

214



215

216 **Fig. 3.** Sample R^2 -frequency relationship for two FRFs [very soft and very strong from test point
217 A1, see Fig. 9 (a)] vs. frequency and corresponding NVI .

218

219 Unless otherwise noted, computations were performed in MATLAB (Mathworks 2020) and plots
220 generated in DPlot (Hyde 2014). Regressions and statistical metrics were computed using
221 STATGRAPHICS (Centurion 2020).

222 3. Numerical Study

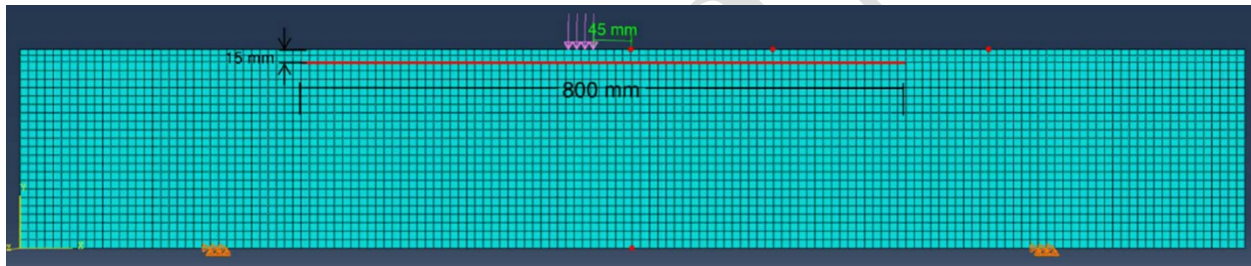
223 3.1. Modeling

224 A plane strain 2D finite element (FE) model was created to simulate the dynamic response of
225 concrete bridge decks with and without delamination theoretically. The objective was to study the
226 effect of a delamination on the dynamic response and whether it causes a nonlinear response. To
227 that end, depth and width of the delamination were selected based on trial and error to prove that
228 the idea works and not necessarily to represent an actual scenario. The bridge deck was modeled
229 as a simply-supported 2D beam using ABAQUS (Systemes 2012) and guided by previous work
230 reported in (Clem, Popovics et al. 2013). The model was created using quadrilateral elements, as
231 shown in Fig. 4. The span length is 1.00 m (39.4 in) and the depth is 240 mm (9.45 in). The material
232 properties assigned to the deck are normal-weight concrete with a modulus of elasticity, $E_c =$
233 23,520 MPa (3,410 ksi) and a mass density, $\rho = 2400 \text{ kg/m}^3$ (150 lb/ft³). An impact force modeled
234 after a typical one observed in the field measurements (see Section 5) was applied as a distributed
235 time-varying force over a length of 40 mm (1.58 in), which corresponds to the diameter of the
236 hammer tip. The forcing function followed a sine (half of a complete cycle) with a duration of 1.8
237 ms. The acceleration response was measured at a point located 45 mm (1.77 in) from the applied
238 impact force.

239
240 Two separate beam models were created: Model 1 refers to the concrete beam without
241 delaminations, i.e., the intact (or reference) beam. Model 2 has the same geometry as Model 1
242 beam but with a delamination, which was modeled as a gap with the following dimensions: Width
243 = 0.5 mm (0.02 in), length = 800 mm (31.5 in), located about the center of the beam at a depth of
244 15 mm (0.59 in) (see Fig. 4). To capture interactions of the delamination boundaries during

245 vibration, these surfaces were modeled as contact elements. In both models, eight impact forces
246 were applied to each of the beams where the peak value of the impact force varied from 0.5 to 15
247 kN (0.112 to 3.37 kip). This range was selected based on the actual forces employed in the field
248 (see Section 5). Note that impact forces reported herein are total force and equivalent distributed
249 forces as applied to the FE models can be calculated as force/0.04 m. A dynamic explicit step
250 routine with a time step of 10 μ s and a total simulation time of 1 s was used. The dynamic response
251 of all 16 simulations was analyzed and is discussed in the following subsection.

252



253

254 **Fig. 4.** Illustration of the 2D finite element (FE) model for Model 2. The red line indicates the
255 delamination (gap). The red point at the surface indicates the acceleration measurement point.

256 The purple arrows indicate the distributed force applied on the deck.

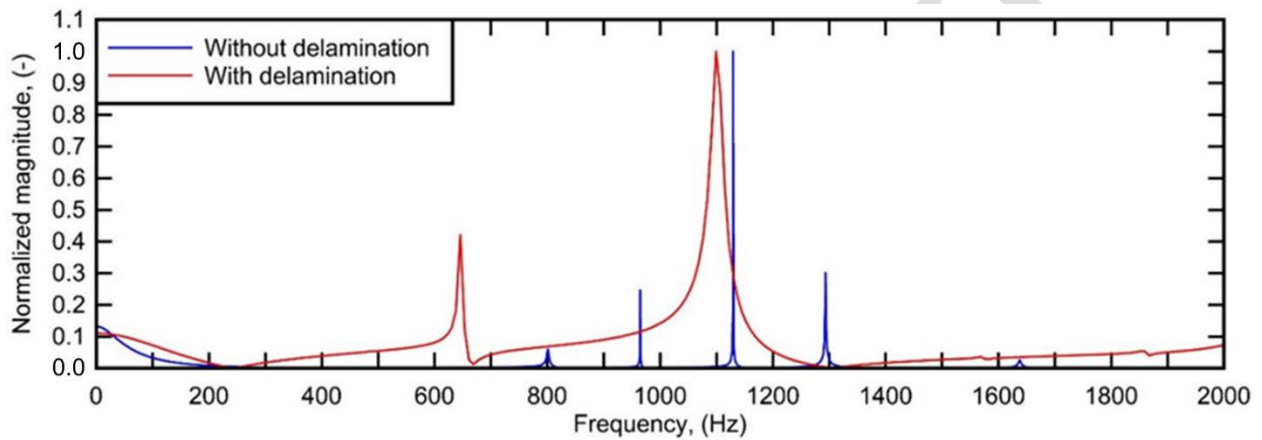
257

258 3.2. Results and Discussion

259 Fig. 5 shows the FRFs of the simulated beams with and without delamination, i.e., Model 2 and
260 Model 1, respectively, due to an impact force with an amplitude of 4 kN (0.9 kip). While it is
261 expected that the natural frequencies of the beam change because of the delamination, the
262 interpretation of the results is not straight forward. As can be seen in Fig. 5, the FRFs look very
263 different for the two models. Not only is there no consistent shift between individual peaks, they

264 also do not have corresponding matches, and exhibit notable differences in their half-power
265 bandwidths. The latter implies higher inherent damping in the system. In conclusion, a
266 delamination has a significant effect on the measured vibration response. However, because the
267 proposed method is self-referencing, this is not relevant.

268

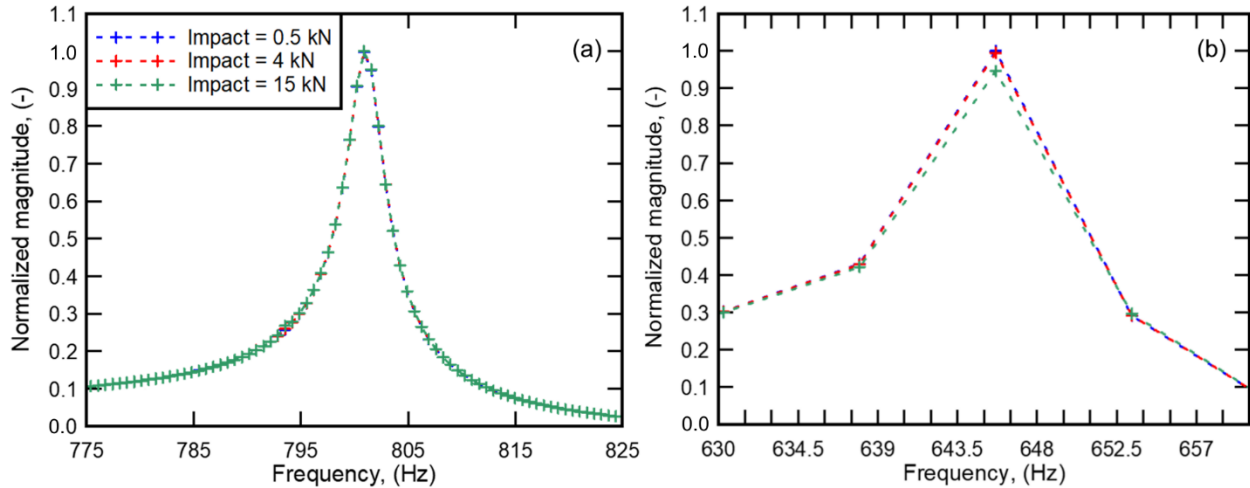


269

270 **Fig. 5.** Two sample FRFs for deck models with and without delamination; amplitude of impact
271 force = 4 kN (0.9 kip).

272

273 As can be observed in Fig. 6 (a), the FRF response of the beam model without delamination for a
274 select peak does not change due to an increasing impact force with amplitudes ranging from 0.5 to
275 15 kN (0.11 to 3.37 kip). On the other hand, increasing the value of the impact force does cause
276 notable changes in the FRFs of the beam model with a delamination. This effect manifests as a
277 change in the magnitude of the selected FRF peaks where the magnitude decreases with increasing
278 impact force, as can be observed in Fig. 6 (b).

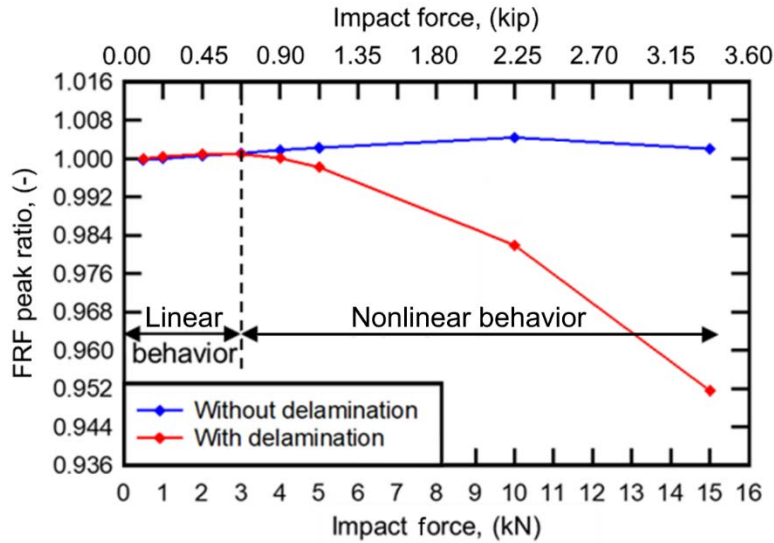


279

280 **Fig. 6.** Three sample FRF peaks (first peak) for impact forces with amplitudes, 0.5, 4 and 15 kN
 281 (0.112, 0.9, and 3.37 kip): (a) Model 1 (without delamination, reference) and (b) Model 2 (with
 282 delamination).

283

284 Fig. 7 shows a comparison of the FRF peak ratios, which corresponds to the FRF peak value
 285 normalized with the FRF peak value for the smallest impact force of 0.5 kN (0.112 kip), for both
 286 beam models. For Model 1 (reference case), it can be observed that there is a minute increase in
 287 the peak response, which can likely be attributed to the nonlinear material response of concrete
 288 (see Section 4.3 for further discussion). Model 2 (delamination case), however, shows a clear
 289 decrease in the peak response after the force exceeds approximately 3 kN (0.674 kip). This
 290 behavior can be associated with contact interaction of the lower and upper boundaries of the
 291 simulated delamination when the vibration amplitude of these boundaries exceeds the width of the
 292 delamination. Our numerical simulations show that changes of the FRF are sensitive to the
 293 presence of a delamination. It can be speculated that other types of damage and degradation have
 294 a similar but smaller effect.

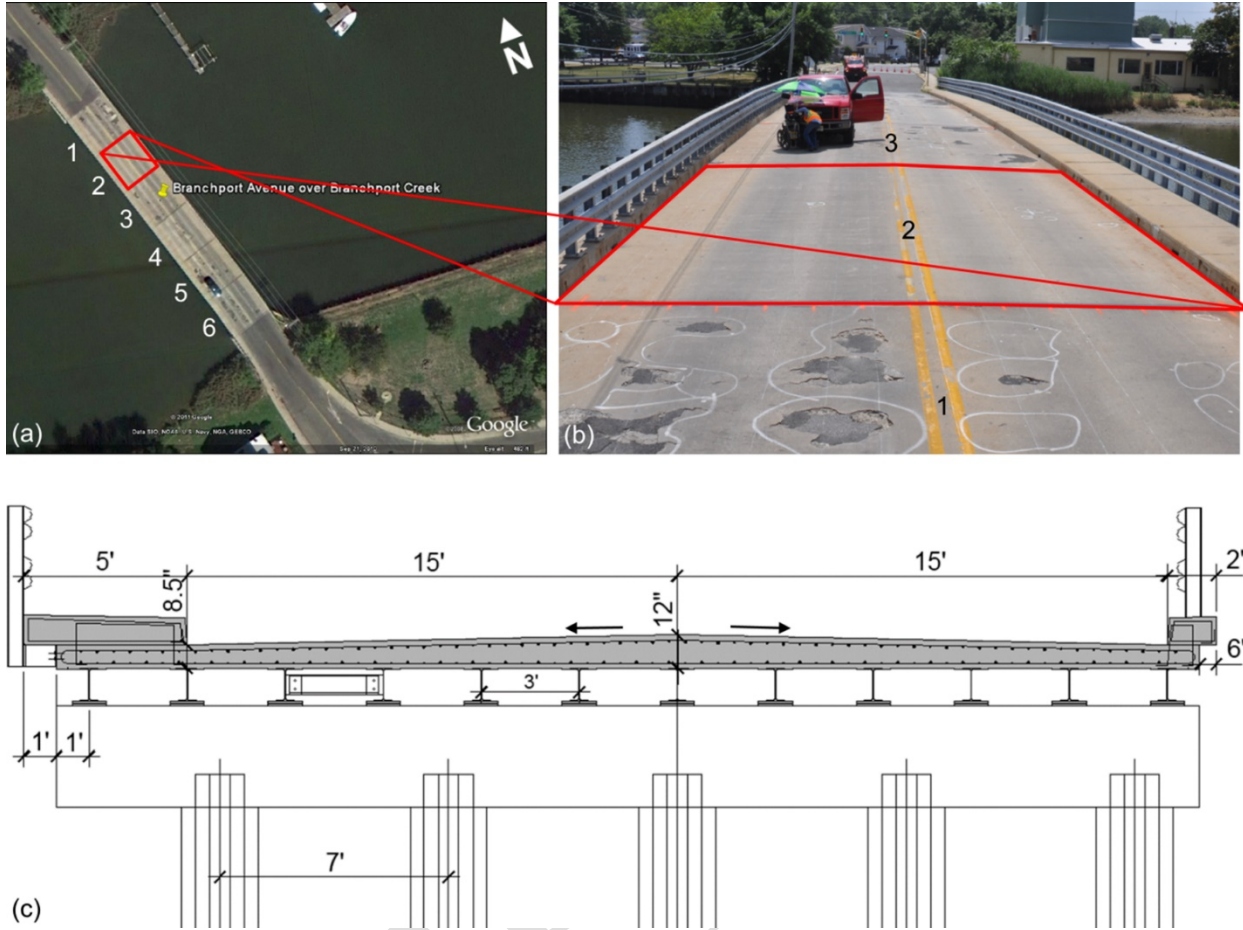


295
296 **Fig. 7.** FRF peak ratio vs. peak impact force value for the two FE models.

297
298 **4. Experimental Study**

299 **4.1. Description of Structure Used for Evaluation**

300 A steel-concrete composite bridge located in Branchport, NJ, USA was selected to evaluate the
 301 proposed method's ability to detect damaged areas in an in-service reinforced concrete bridge
 302 deck. The bridge, presented in Fig. 8, has a total length of 65.8 m (216 ft) and is 11.3 m (37 ft)
 303 wide. The superstructure consists of six 11.0 m (36 ft) long two-span sections with steel girders
 304 carrying a 216 to 305 mm (8.5 to 12 in) thick reinforced concrete deck, as shown in Fig. 8 (c). Due
 305 to the harsh environment combined with exposure to chlorides from seawater and deicers, the
 306 bridge exhibited severe distress when it was visually inspected in July 2011. Five of the six deck
 307 sections were found to have severe surface damage, showing visible signs of spalling, potholes,
 308 and in some locations the steel rebars were exposed. The deck selected for this study (#2,
 309 highlighted in Figs. 8 (a) and b) showed no visual distress and hammer sounding revealed only
 310 two small areas potentially having delaminations [see Fig. 9 (a)].



311 (c)

312 **Fig. 8.** Branchport Avenue Bridge in Long Branch, NJ: (a) Google map image showing plan
 313 view and selected deck (#2) used as part of this study, (b) photo of Deck #2 from a driver's
 314 perspective, and (c) bridge cross-section with dimensions in (in = \" and (ft = \"). Unit
 315 conversion: 1 in = 25.4 mm, 1 ft = 0.305 m.

316

317 Since the responsible County had planned to rehabilitate the entire bridge deck, this represented
 318 an opportunity to evaluate a variety of NDT methods by comparing their results with the removed
 319 concrete. Findings are reported in Clem (Clem 2013) and Celaya et al. (Celaya, Schumacher et al.
 320 2014). The NDT surveys, including the IR testing discussed in this article, were completed in July
 321 2011; hydro-blasting to remove surface as well as damaged concrete was performed in March

322 2013. Before new concrete was placed in July 2013, the depth of the removed concrete was
323 measured on a 610 x 610 mm (2 x 2 ft) grid. Depth measurements were established using traditional
324 surveying equipment and made available by Cherry, Weber & Associates.

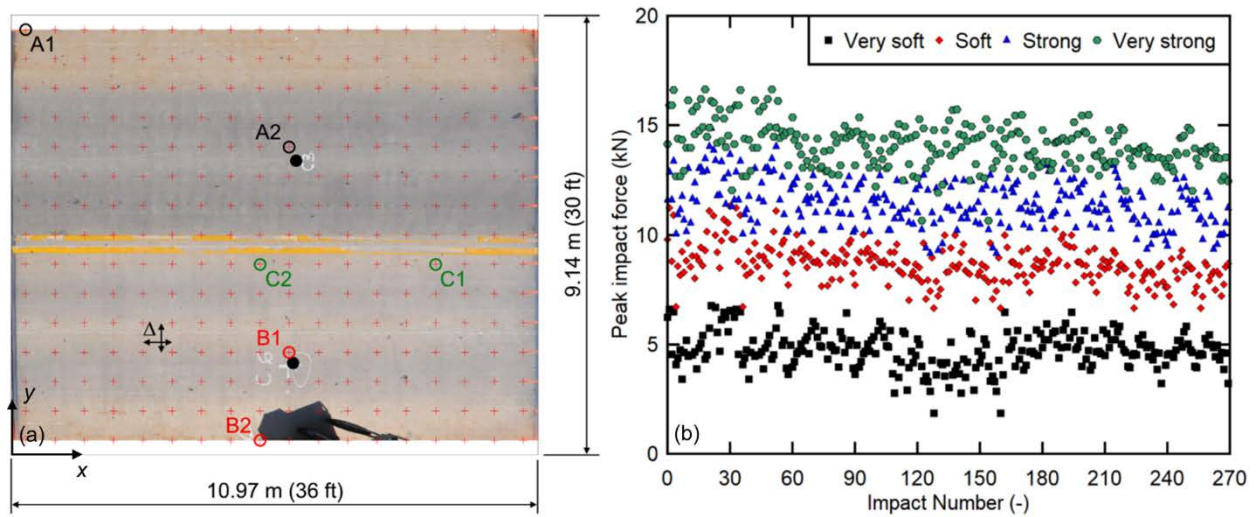
325

326 **4.2. Test Setup and Procedure**

327 A typical impulse response (IR) test setup was used, as illustrated in Fig. 1. The hammer (PCB,
328 Model 086D20) weighs 0.67 kg (1.5 lb) and has a 51 mm (2 in) diameter hard-plastic hammer tip
329 [± 22.2 kN-peak (5000 lb-peak)]. It is equipped with a piezoelectric load cell connected to a signal
330 amplifier/conditioner to measure the generated impact force. The vibration response was measured
331 using a capacitive MEMS accelerometer (Silicon Designs-Model-2260-010) that has a flat frequency
332 response within 3 dB over the range of 0 to 1 kHz. Both input (force) and output (acceleration)
333 signals were recorded using a high-speed transient recorder (Elsys, Model TraNET 204s) with a
334 sampling frequency of 500 kHz.

335

336 The two-lane traffic portion of Deck #2, measuring 9.14 x 11.0 m (30 x 36 ft), was divided into a
337 610 x 610 mm (2 x 2 ft) test grid, resulting in 270 individual test points, as shown in Fig. 9 (a).
338 Two locations were selected for concrete coring and are highlighted by solid black circles. Four
339 hammer impacts were applied at each test point manually, i.e., by a human operator, with increasing
340 amplitude, referred to as “very soft”, “soft”, “strong”, and “very strong”, as illustrated in Fig. 9 (b).
341 Sample results from the proposed test method are shown as colored circles and marked A1, A2, B1,
342 B2, C1, C2 [see Fig. 9 (a)] and are discussed in detail in Section 6.1.



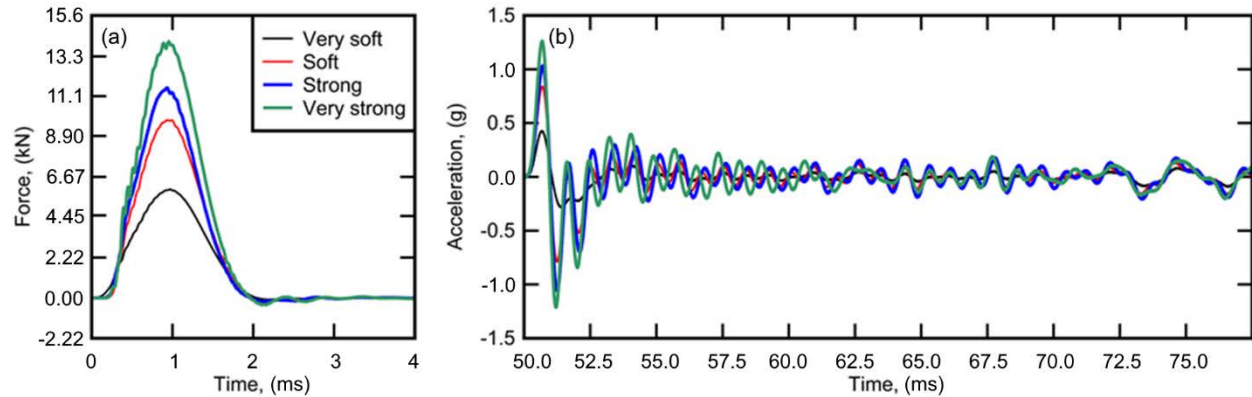
343

344 **Fig. 9.** (a) Plan view photo of Deck #2 with test grid (red '+'), $\Delta = 0.61$ m (2 ft), locations of
 345 sample test points A1, A2, B1, B2, C1, and C2, and extracted concrete cores (full black circles).

346 (b) Peak impact forces for all 270 test points. Unit conversion: 20 kN = 4.5 kip.

347

348 Fig. 10 shows sample time histories of four impact forces with different levels of amplitude and
 349 the corresponding acceleration responses for one select test point.



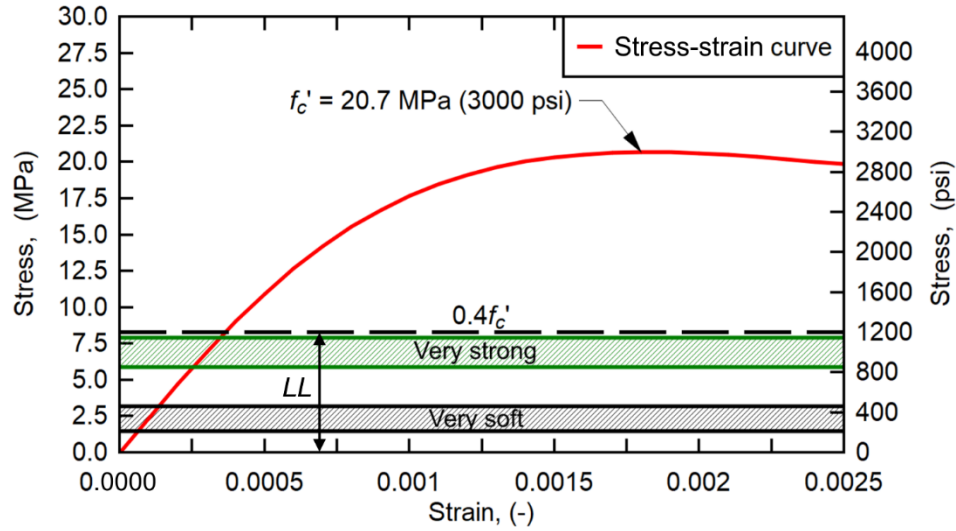
350

351 **Fig. 10.** Samples of (a) four impact forces and (b) corresponding acceleration responses for one
 352 select test point. Unit conversion: 15.6 kN = 3.5 kip.

353

354 4.3. Sources of Nonlinearity

355 Structural systems may exhibit nonlinear vibrations due to several factors (Farrar and Worden
 356 2013). For the system investigated in this study, two factors are considered: Material nonlinearity
 357 and crack boundary interaction. The former is due to the nonlinear stress-strain relationship of
 358 concrete. To ensure that our proposed *NVI* is not affected by this nonlinearity, the stresses
 359 generated from the impact forces were calculated and compared with the theoretical concrete
 360 stress-strain relationship proposed by Carreira and Chu (Carreira and Chu 1985). Fig. 11 shows
 361 this stress-strain relationship, which assumes a conservative concrete compressive strength, $f_c' =$
 362 20.7 MPa (3,000 psi). It can be observed that all generated stresses lie within the suggested linear
 363 limit (*LL*) of 40% of f_c' (shown as black dashed line) (fib 2010). The ranges of generated stresses
 364 for “very soft” and “very strong” impact forces spanning the means +/- two standard deviations
 365 taken from data shown in Fig. 9 (b) are provided for reference. To conclude, effects due to material
 366 nonlinearity can be assumed to have a negligible effect on the proposed nonlinearity parameter,
 367 *NVI*.



368

369 **Fig. 11.** Theoretical Stress-Strain relationship and actual generated stress ranges due to “very
 370 soft” (grey area) and “very strong” (green area) impact forces (ranges span mean +/- two
 371 standard deviations). The black dashed horizontal line represents the suggested linear limit (*LL*).

372

373 Cracks resulting from concrete degradation is the second factor leading to nonlinearity, and of
 374 interest to this study. Cracks open and close during vibrations, leading to a complex dynamic
 375 response when the crack boundaries interact, which has been referred to as crack breathing
 376 (Giannini, Casini et al. 2014). Although the cracks are initially small and distributed, they may
 377 grow and coalesce to eventually form a localized macro crack such as a shallow delamination in a
 378 concrete bridge deck. As demonstrated in Section 3, the proposed *NVI* should theoretically be able
 379 to detect this type of damage. While a delamination is distinctly different from distributed micro
 380 cracks, the crack breathing model still applies; in fact, it can be hypothesized that it is much more
 381 pronounced for this case.

382 To conclude, since material nonlinearity is deemed negligible, only cracking-related degradation
383 should affect the *NVI*. Furthermore, it is assumed that the stress-strain relationship does not have
384 a notable effect on detectability of concrete degradation such as a delamination.

385

386 **5. Results and Discussion**

387 **5.1. Verification of Results from Individual Test Points**

388 As has been reported, the crack boundary interaction of a delamination can cause nonlinear
389 vibrations due to the effects of the crack breathing phenomenon (Giannini, Casini et al. 2014). In
390 this section, results from six test points on Deck #2 were selected and are discussed in detail to
391 evaluate the proposed test method. The six test points were divided into three groups (A, B, and
392 C) according to the observed results from the proposed method, available cores, and visual
393 inspection (see Fig. 9 (a) for test point locations). Each group consists of two test points (see Table
394 1). Note that “very soft” serves as the reference case for the three other impact forces, namely
395 “soft”, “strong”, and “very strong”. The level of nonlinearity of the tested locations, which is
396 represented by the *NVI*, was computed over a frequency range of $f_1 = 225$ to $f_2 = 500$ Hz. The lower
397 limit, f_1 of this subjective range was chosen to exclude low-frequency noise caused by traffic,
398 wind, etc. The upper limit, f_2 was selected to minimize the effect of nonlinearity introduced by the
399 used accelerometer. In a previous study the authors used the same instrumentation and found this
400 type of nonlinear vibration response to start at approximately 600 Hz (Hafiz and Schumacher
401 2019). Therefore, the upper limit was conservatively set at 500 Hz.

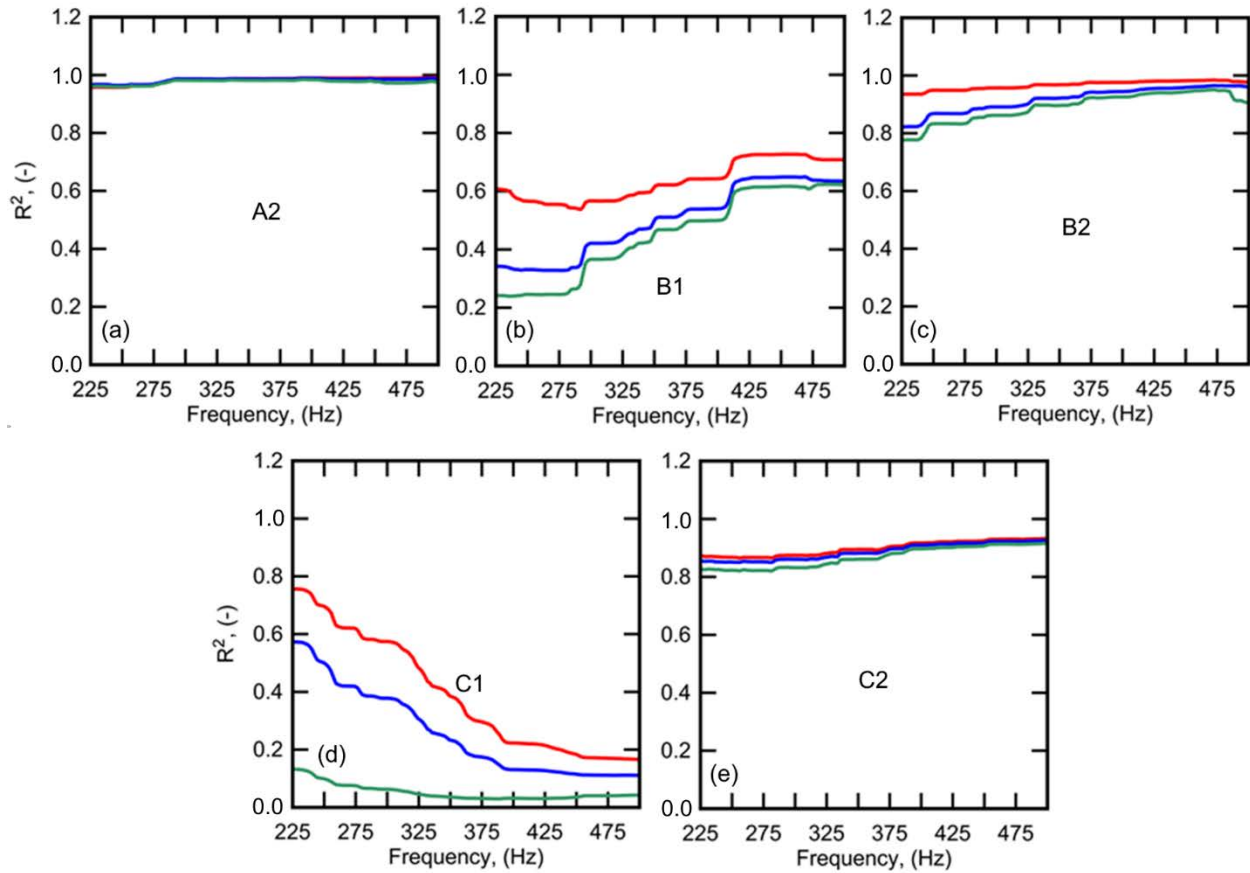
402

Table 1. Six selected test point coordinates and their *NVI*; “very soft” = reference case.

Group	Location [see Fig. 9 (a)]	x [m (ft)]	y [m (ft)]	<i>NVI</i> (-)		
				Soft	Strong	Very strong
A	A1	0.305 (1.00)	8.84 (29.0)	0.99	0.98	0.98
	A2	5.79 (19.0)	6.40 (21.0)	0.98	0.98	0.97
B	B1	5.79 (19.0)	2.13 (7.00)	0.63	0.49	0.44
	B2	5.18 (17.0)	0.305 (1.00)	0.96	0.91	0.98
C	C1	8.84 (29.0)	3.96 (13.0)	0.38	0.25	0.05
	C2	5.18 (17.0)	3.96 (13.0)	0.89	0.88	0.86

403

404 Group A represents two test points that were not found to have any form of degradation by visual
405 inspection. Fig. 2 shows the FRF for test point A1, as well as the peak impact forces. Recall from
406 the discussion in Section 3, although the impact force was more than doubled, this only had a very
407 minor effect on the FRF, which implies the system is linear. Fig. 3 shows the R^2 -frequency
408 relationship for test point A1, which is close to 1, indicating near linear behavior. Similarly, the
409 R^2 -frequency relationship of test point A2 is also not significantly affected by the increase of the
410 impact force, as can be observed in Fig. 12 (a). Since any structure will demonstrate a certain level
411 of nonlinearity, 3% can be interpreted as the uncertainty in the *NVI* value for non-degraded
412 concrete in this study. The concrete core taken near test point A2 is further proof that this location
413 is in healthy condition, i.e., not showing any delamination, as can be seen in Fig. 13 (a). In
414 conclusion, areas on the bridge deck that do not show signs of nonlinear vibration behavior can be
415 considered healthy, i.e., free of degradation or delaminations, which supports the basic idea behind
416 our proposed method.



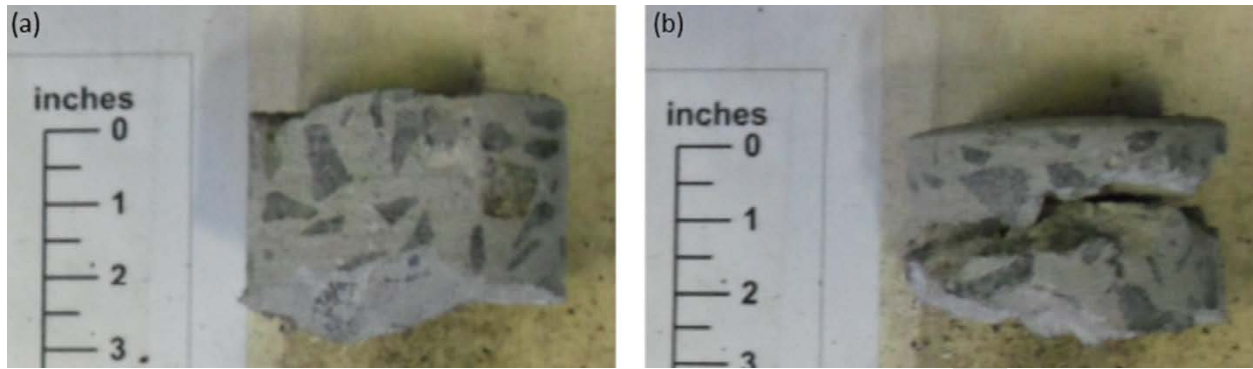
417

418 **Fig. 12.** R^2 - frequency relationships for test point A2 (a), B1 (b), B2 (c), C1 (d), and C2 (e).

419 Locations of these test points are shown in Fig. 9(a). Photos of extracted cores corresponding to

420 (a) and (b) are shown in Fig. 13. Note that the R^2 - frequency relationships for test point A1 is

421 shown in Fig. 3.



422

423 **Fig. 13.** Photos of extracted concrete cores: (a) Core 1 (near A2) and (b) Core 2 (near B1).

424

425 Group B represents two test points that were marked having delaminations by means of chain drag.

426 The R^2 - frequency relationships for the Group B test points are presented in Figs. 12 (b) and (c). It

427 can be observed that the responses are significantly affected with increasing impact force, leading

428 to low R^2 functions. Additionally, along with an increase in the amplitude of the impact force, the

429 change in the R^2 - frequency relationship increases, resulting in a decrease in the NVI value, as

430 shown in Table 1. This response is distinctly different from the one found in Group A. These

431 results also match the core taken near test point B1, which shows a horizontal crack at a depth of

432 approximately 25 mm (1 in) [see Fig. 13 (b)]. In conclusion, the Group B results further confirm

433 that our proposed method can detect delaminations. The NVI values for test point B2 are not as

434 low as for B1, which is where visual inspection found a small, delaminated area [see Fig. 9 (a)].

435

436 Group C represents two test locations that exhibited nonlinear vibration behavior, but where the

437 visual inspection did not find any degradation or delaminations. The two associated test points

438 exhibited strong nonlinear vibration behavior, as shown in their FRFs [see Figs. 12 (d) and (e)].

439 Unfortunately, no cores were available for the Group C test locations. However, the NVI values

440 could be compared with the depth of the removed concrete after hydro-blasting was performed,
441 which is discussed in more detail in Section 6.2. The depth of removed concrete for these locations
442 was approximately 40 mm (1.6 in) for C1 and C2, which can be considered relatively high.
443 Assuming that hydro-jetting removes more depth when the concrete is degraded, i.e., having
444 distributed micro cracks, the hypothesis that the *NVI* method can detect degradation is also
445 supported.

446

447 Since only two cores were available for the entire deck, a comparison between the *NVI* results and
448 the depth of removed concrete was the only way to evaluate the proposed method for all 270 test
449 points, which is discussed in the subsequent section.

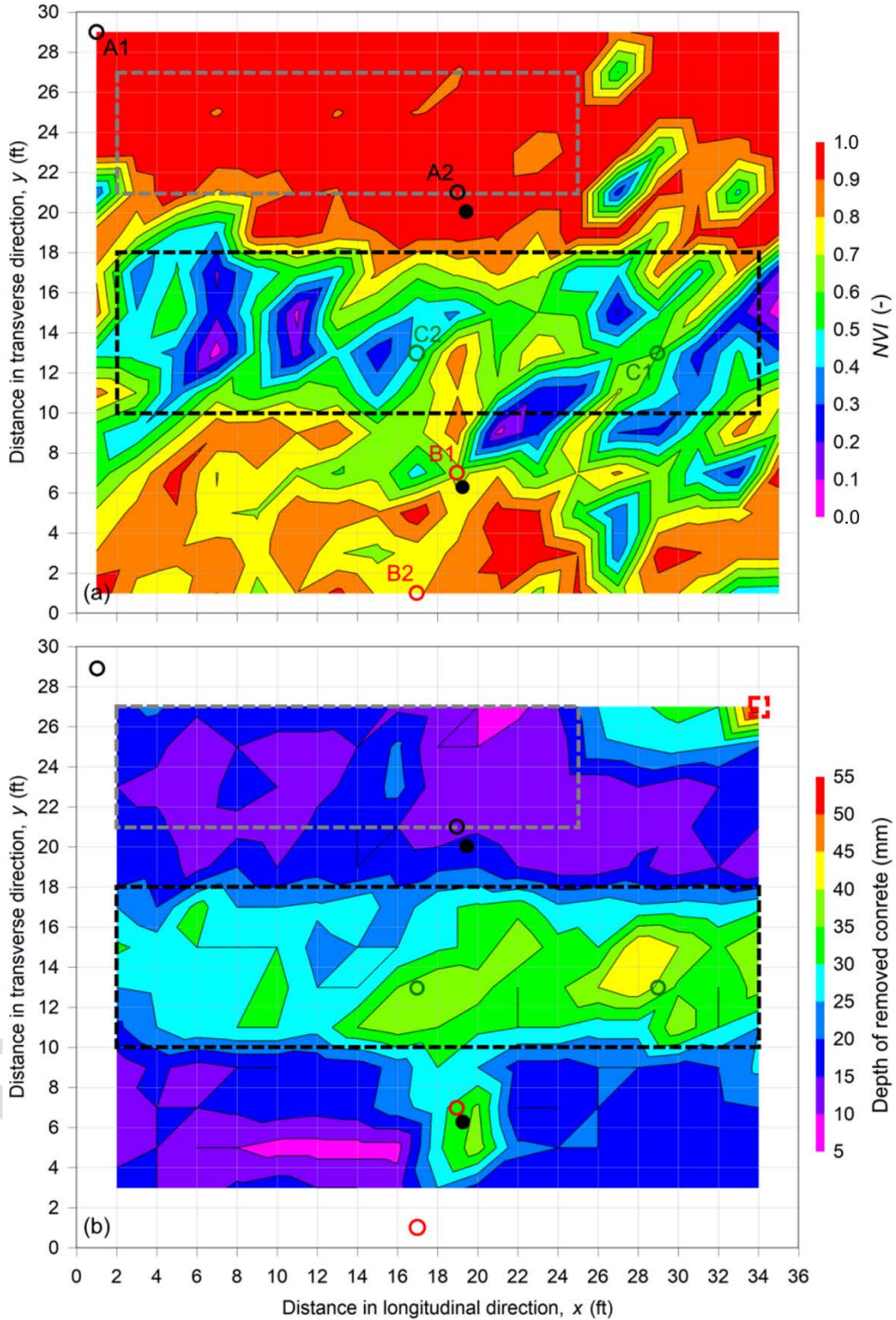
450

451 **5.2. Comparison of Results with Removed Concrete**

452 Fig. 14 shows contour plots of (a) *NVI* values and (b) depth of removed concrete by hydro-blasting
453 across the entire Deck #2. *NVI* values were computed between the “very soft” (= reference) and
454 “very strong” impact forces. Both *NVI* results and depth of removed concrete agree in that there is
455 a large degraded or delaminated area along the centerline of the deck as highlighted by the black
456 dashed box. Additionally, both figures show that the area highlighted by the gray dashed boxes
457 are in good condition. On the other hand, the *NVI* method missed a literal hole in the deck found
458 after hydro-blasting had been completed, as highlighted by the red dashed box. This, however,
459 makes sense, since a hole is simply the case of material missing in some area, which is not the
460 same as an area of degraded concrete. Also, several low *NVI* values, e.g., around $x = 5.49$ to 6.71
461 m (18 to 22 ft) and $y = 0.91$ to 2.13 m (3 to 7 ft), which would point to degradation or delamination,
462 are visible that could not be associated with a high depth of removed concrete. Note that the *NVI*

463 value for test point B1 was consistent with the nearby concrete core that was found to have a
464 delamination, as is discussed in Section 5.1. The discrepancy away from this test point highlights
465 the need for additional work to better understand other factors not yet considered.

PREPRINT

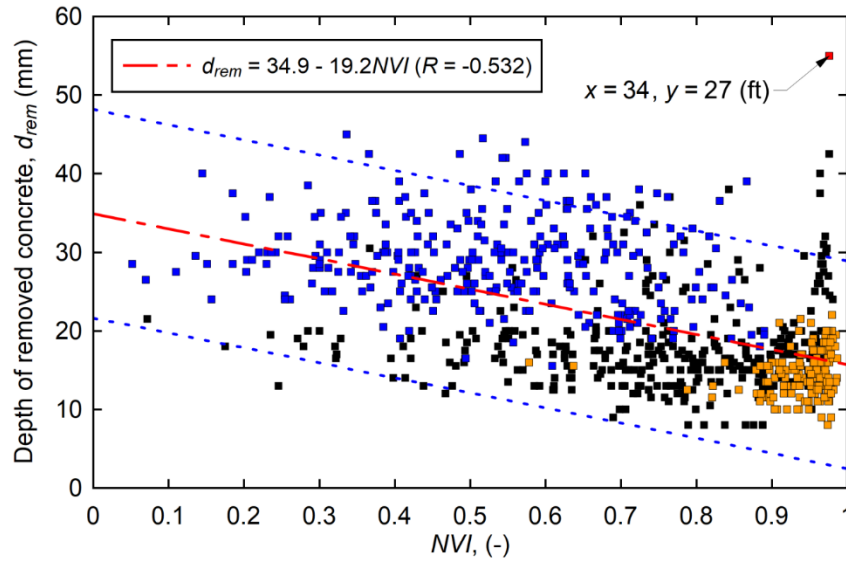


466

467 **Fig. 14.** Contour plots for (a) NVI values and (b) depth of removed concrete for Deck #2. Circles

468 depict select test points discussed in more detail in Section 5.1. Unit conversion: 1 ft = 0.305 m.

469 Fig. 15 shows a correlation plot between *NVI* values and depth of removed concrete. The data
470 behind this plot were generated by interpolating the two datasets shown Fig. 14 over a range $x =$
471 0.610 to 10.4 m (2 to 34 ft) and $y = 0.914$ to 8.23 m (3 to 27 ft) using the generate mesh function
472 with planar interpolation available in DPlot (Hyde 2014). Linear least-squares regression was
473 performed on these data to determine the mean prediction curve (red dash-dotted line) and 95%
474 prediction limits (blue dotted lines). While a linear relationship with statistical significance at the
475 95% confidence level exists, the correlation coefficient, $R = -0.532$ is low and considerable scatter
476 is present. As such, this relationship should only be interpreted as an indication of an overall trend.
477 Orange and blue dots correspond to data points from within the grey and black dashed boxes,
478 respectively, shown in Fig. 14, and the red dot corresponds to the location of the hole discussed
479 earlier [at $x = 10.4$ m (34 ft), $y = 8.23$ m (27 ft)]. While it can be concluded that the *NVI* cannot be
480 directly used to predict the amount of removed concrete during hydro-blasting, Fig. 15 nonetheless
481 indicates that our proposed method is not only capable of detecting the onset of delaminations but
482 may also be sensitive to distributed damage. Note that a data analysis following conventional IR
483 parameters (ASTM 2016) did not reveal any of these issues (Clem 2013).



484

485 **Fig. 15.** *NVI* - Depth of removed concrete vs. *NVI* correlation plot. Orange and blue dots
 486 correspond to data points from within the grey and black dashed boxes, respectively, shown in
 487 Fig. 14. The red dash-dotted line and blue dotted lines represent the mean prediction curve and
 488 95% prediction limits, respectively. Unit conversion: 1 ft = 0.305 m.

489

490 6. Summary and Conclusions

491 The presented results demonstrate the potential for our proposed nonlinear vibration index (*NVI*)
 492 method to detect degradation and delamination in reinforced concrete bridge decks. The *NVI*
 493 method is based on the concept of deviation from linearity, which is determined by computing the
 494 frequency response functions (FRFs) for a set of increasing impact forces applied to a specific test
 495 point and comparing them via correlation coefficients. The hypothesis is that if the FRFs remain
 496 constant and change, this can be associated with healthy and degraded or damaged areas,
 497 respectively. A numerical study using a finite element (FE) model demonstrated that nonlinear
 498 behavior was indeed exhibited for a deck with a delamination when subject to increasing impact

499 forces. The proposed method was then evaluated using data from an in-service bridge deck. The
500 equipment is the same as is used for impulse response (IR) tests on concrete plates. The results of
501 the field study support the proposed hypothesis. A comparison between *NVI* results and visual
502 inspection results, extracted concrete cores for six test locations, as well as depth of removed
503 concrete from hydro-blasting was performed. The final observations and conclusions are as
504 follows:

- 505 • *NVI* results were able to distinguish healthy areas in the bridge deck with ones that had
506 degradation or delaminations. Additionally, *NVI* results were in excellent agreement with
507 visual inspection and core test results.
- 508 • A strong match was found between the results of the *NVI* method and visual inspection and
509 cores for detecting areas that could potentially have degradation or delamination.
- 510 • A qualitative comparison between *NVI* values and depth of removed concrete showed
511 acceptable agreement in terms of areas of degradation or delaminations.
- 512 • An overall trend was found between *NVI* values and depth of removed concrete. While notable
513 scatter exists, a linear regression revealed a trend consistent with the proposed hypothesis. Note
514 that the mean prediction equation found through linear least-squares regression should not be
515 used to predict depth of removed concrete.

516

517 It should be noted that the proposed method, at this point, cannot distinguish between type of
518 damage. Additional research is required before predictions with respect to type of damage and
519 depth of removed concrete can be made reliably. Future work includes additional modeling and
520 laboratory work to establish firm relationships as well as define the limitations of the method. For

521 example, additional scenarios should be studied where crack depth, crack extent, applied force,
522 etc. are varied, to ensure the method works under many possible configurations in the field.

523

524 **7. Acknowledgments**

525 The authors thank The Higher Committee for Education Development in Iraq for supporting the
526 first author. Test equipment was made available by the Department of Civil and Environmental
527 Engineering at the University of Delaware. The data analyzed in this article were collected as part
528 of a research project sponsored by the Delaware Department of Transportation. We thank Dr.
529 Lassaad Mhamdi, Daniel J. Clem, Tayler C. Wennick, and Kaitlyn N. Gisonda for assisting with
530 data collection. Access to the bridge as well as traffic management during testing was provided by
531 Dr. Kaz Tabrizi and Dr. Manuel Celaya from Advanced Infrastructure Designs and Greg Bitsko
532 from Cherry, Weber & Associates, and are greatly appreciated.

533

534 **8. References**

- 535 Abdelkhalek, S. and T. Zayed (2020). "Comprehensive Inspection System for Concrete Bridge
536 Deck Application: Current Situation and Future Needs." ASCE Journal of Constructed
537 Facilities **34**(5): 03120001.
- 538 Arndt, R. W., T. Schumacher, D. Algernon and S.-H. Kee (2011). "Strategies for maintenance of
539 highway bridges in the U.S. - with the support of non-destructive testing and structural health
540 monitoring." Bautechnik **88**(11): 793-804.
- 541 ASTM (2016). C1740: Standard Practice for Evaluating the Condition of Concrete Plates Using
542 the Impulse-Response Method. West Conshohocken, PA, ASTM International.

543 Bien, J., J. Krzyzanowski, W. Poprawski, W. Skoczynski and J. Szymkowski (2002). Experimental
544 study of bridge structure dynamic characteristics using periodic excitation. International
545 Conference on Noise and Vibration Engineering. Leuven, Belgium. **II**: 555-562.

546 Carreira, D. J. and K.-H. Chu (1985). "Stress-Strain Relationship for Plain Concrete in
547 Compression." ACI Journal Proceedings **82**(6): 797-804.

548 Celaya, M., T. Schumacher, K. Tabrizi, G. Bitsko and P. Shokouhi (2014). Field Verification of
549 Non-destructive Testing Technologies for Condition Assessment of Concrete Bridge Decks:
550 A Case Study. NDE/NDT for Structural Materials Technology for Highway & Bridges.
551 Washington, D.C., ASNT.

552 Centurion, S. (2020). STATGRAPHICS. The Plains, VA, Statgraphics Technologies, Inc.

553 Clem, D. J. (2013). Evaluation of impulse response & ground-penetrating radar as a means of non-
554 destructive testing of concrete bridge decks. M.S. Thesis. Newark, DE, University of
555 Delaware.

556 Clem, D. J., J. S. Popovics, T. Schumacher, T. Oh, S. Ham and D. Wu (2013). Understanding the
557 impulse response method applied to concrete bridge decks. Review of Progress in Quantitative
558 Nondestructive Evaluation. Denver, CO, AIP Conference Proceedings. **1511**: 1333-1340.

559 Davis, A. G. (2003). "The nondestructive impulse response test in North America: 1985-2001."
560 NDT & E International **36**(4): 185-193.

561 Davis, A. G. and C. Germann Petersen (2003). Nondestructive Evaluation of Prestressed Concrete
562 Bridges using Impulse Response. Non-Destructive Testing in Civil Engineering 2003. Berlin,
563 Germany, NDT.net.

564 Davis, A. G. and S. A. Robertson (1975). "Economic Pile Testing." Ground Engineering **8**(3): 40-
565 43.

566 Doebling, S. W., C. R. Farrar and M. B. Prime (1998). "A Summary Review of Vibration-Based
567 Damage Identification Methods." The Shock and Vibration Digest.

568 Ewins, D. J. (1995). Modal Testing: Theory and Practice. New York, John Wiley & Sons Ltd.

569 Farrar, C. R. and K. Worden (2013). Structural Health Monitoring: a Machine Learning
570 Perspective. West Sussex, UK, John Wiley & Sons, Ltd.

571 fib (2010). Model Code for Concrete Structures.

572 Garrett, S. (2019). "Nondestructive Assessment of Bridge Decks." Materials Evaluation **77**(4).

573 Giannini, O., P. Casini and F. Vestroni (2014). "Nonlinear Harmonic Identification of Cracks in
574 Structures." Dynamics of Civil Structures **4**: 207-217.

575 Gucunski, N., A. Imani, F. Romero, S. Nazarian, Y. Deren, H. Wiggengerhauser, P. Shokouhi, A.
576 Taffe and D. Kutrubes (2013). Nondestructive Testing to Identify Concrete Bridge Deck
577 Deterioration. Washington, D.C., Transportation Research Board.

578 Hafiz, A. and T. Schumacher (2019). "Effects of Elastic Supports and Flexural Cracking on Low
579 and High Order Modal Properties of a Reinforced Concrete Girder." Engineering Structures
580 **178**: 573-585.

581 Hyde, D. (2014). DPlot. Vicksburg, MS, HydeSoft Computing LLC.

582 Idriss, M., A. El Mahi and R. El Guerjouma (2015). "Characterization of Sandwich Beams with
583 Debonding by Linear and Nonlinear Vibration Method." Composite Structures **120**: 200-207.

584 Kee, S.-H. and N. Gucunski (2016). "Interpretation of Flexural Vibration Modes from Impact-
585 Echo Testing." ASCE Journal of Infrastructure Systems **22**(3): 04016009.

586 Kee, S.-H., T. Oh, J. S. Popovics and R. W. Arndt (2012). "Nondestructive Bridge Deck Testing
587 with Air-Coupled Impact-Echo and Infrared Thermography." ASCE Journal of Bridge
588 Engineering **17**(6): 928-939.

589 Kerschen, G., K. Worden, A. F. Vakakis and J.-C. Golinval (2006). "Past, Present and Future of
590 Nonlinear System Identification in Structural Dynamics." Mechanical Systems and Signal
591 Processing **20**(3): 505-592.

592 Lin, R. (1990). Identification of the Dynamic Characteristics of Nonlinear Structures. PhD,
593 University of London.

594 Lin, S., H. Azari, D. Meng and S. Shams (2021). Nondestructive Evaluation of Concrete Bridge
595 Decks with Overlays. Washington, D.C., FHWA Turner-Fairbank Highway Research Center.

596 Liu, C.-J., M. D. Todd, Z.-L. Zheng and Y.-Y. Wu (2017). "A Nondestructive Method for the
597 Pretension Detection in Membrane Structures Based on Nonlinear Vibration Response to
598 Impact." Structural Health Monitoring **17**(1): 67-79.

599 Mathworks (2020). MATLAB. Natick, MA, Mathworks.

600 NCHRP (2004). Concrete Bridge Deck Performance - A Synthesis of Highway Practice. NCHRP
601 Synthesis 333. Washington, D.C., Transportation Research Board.

602 Noel, J. P. and G. Kerschen (2017). "Nonlinear System Identification in Structural Dynamics: 10
603 More Years of Progress." Mechanical Systems and Signal Processing **83**: 2-35.

604 Sajid, S. and L. Chouinard (2019). "Impulse response test for condition assessment of concrete: a
605 review." Construction and Building Materials **211**: 317-328.

606 Salawu, O. S. and C. Williams (1995). "Bridge Assessment Using Forced-Vibration Testing."
607 ASCE Journal of Structural Engineering **121**(2): 161-173.

608 Samman, M. M. and M. Biswas (1994). "Vibration Testing for Nondestructive Evaluation of
609 Bridges. I: Theory." ASCE Journal of Structural Engineering **120**(1): 269-289.

610 Samman, M. M. and M. Biswas (1994). "Vibration Testing for Nondestructive Evaluation of
611 Bridges. II: Results." ASCE Journal of Structural Engineering **120**(1): 290-306.

612 Sansalone, M. J. and W. B. Streett (1997). Impact-Echo - Nondestructive Evaluation of Concrete
613 and Masonry. Ithaca, NY, Bullbrier Press.

614 Scherr, J. F. and C. Grosse (2021). "Delamination detection on a concrete bridge deck using impact
615 echo scanning." Structural Concrete **22**(2): 806-812.

616 Scott, M., A. Rezaizadeh, A. Delahaza, C. G. Santos, M. Moore, B. Graybeal and G. Washer
617 (2003). "A Comparison of Nondestructive Evaluation Methods for Bridge Deck Assessment."
618 NDT & E International **36**(4): 245-255.

619 Shokouhi, P., J. Wolf and H. Wiggenhauser (2014). "Detection of Delamination in Concrete
620 Bridge Decks by Joint Amplitude and Phase Analysis of Ultrasonic Array Measurements."
621 ASCE Journal of Bridge Engineering **19**(3): 04013005.

622 Sun, H., J. Zhu and S. Ham (2018). "Automated Acoustic Scanning System for Delamination
623 Detection in Concrete Bridge Decks." ASCE Journal of Bridge Engineering **23**(6): 04018027.

624 Systemes, D. (2012). ABAQUS 6.12.

625 Underwood, S. S., J. J. Meyer and D. E. Adams (2015). "Damage Localization in Composite
626 Structures Using Nonlinear Vibration Response Properties." Journal of Vibration and
627 Acoustics **137**(3): 031015.

628 Zhang, G., R. S. Harichandran and P. Ramuhalli (2012). "Automatic Delamination Detection of
629 Concrete Bridge Decks Using Impact Signals." ASCE Journal of Bridge Engineering **17**(6):
630 951-954.

631 Zhao, X. Y., Z.-Q. Lang, G. Park, C. R. Farrar, M. D. Todd, Z. Mao and K. Worden (2015). "A
632 New Transmissibility Analysis Method for Detection and Location of Damage via Nonlinear
633 Features in MDOF Structural Systems." IEEE/ASME Transactions on Mechatronics **20**(4):
634 1933-1947.

- 635 Zhou, H. F., Y. Q. Ni and J. M. Ko (2011). "Eliminating Temperature Effect in Vibration-Based
636 Structural Damage Detection." ASCE Journal of Engineering Mechanics **137**(12): 785-796.
- 637 Zhou, Z., L. D. Wegner and B. F. Sparling (2007). "Vibration-Based Detection of Small-Scale
638 Damage on a Bridge Deck." ASCE Journal of Structural Engineering **133**(9): 1257-1267.

PREPRINT